Improvement of near-infrared (NIR) reflectivity and black color tone by doping Zn^{2+} into the $Ca_2Mn_{0.85}Ti_{0.15}O_4$ structure

Ryohei Oka,[a] Senri Iwasaki[b] and Toshiyuki Masui [ID] *[bc]

Inorganic black pigments with thermal barrier characteristics, $Ca_2Mn_{0.85-x}Ti_{0.15}Zn_xO_{4-x}$ ($0 \leq x \leq 0.10$), were synthesized using a conventional solid-state reaction method in order to improve the blackness without decreasing the near-infrared (NIR) reflectance of a $Ca_2Mn_{0.85}Ti_{0.15}O_4$ pigment, which was previously reported by our group. The composition was optimized to provide both high blackness and NIR reflection characteristics. As a result, the NIR solar reflectance value (R_{NIR}) of $Ca_2Mn_{0.77}Ti_{0.15}Zn_{0.08}O_{3.92}$ ($R_{NIR} = 74.6\%$) became larger than that of $Ca_2Mn_{0.85}Ti_{0.15}O_4$ ($R_{NIR} = 71.7\%$), and the black color tone of the former ($L^* = 23.2$, $a^* = +2.81$, $b^* = +0.83$, $C = 2.93$) was improved in comparison with that of the latter ($L^* = 24.4$, $a^* = +4.30$, $b^* = +2.72$, $C = 5.09$). This improvement is caused by the introduction of strain into the $[MnO_6]$ octahedra and a decrease in the manganese ion concentration. The R_{NIR} value of the $Ca_2Mn_{0.77}Ti_{0.15}Zn_{0.08}O_{3.92}$ pigment was also larger than those of the commercially available pigments ($R_{NIR} < 53.0\%$). Therefore, $Ca_2Mn_{0.77}Ti_{0.15}Zn_{0.08}O_{3.92}$ has potential to be an inorganic black pigment for thermal shielding.

Introduction

The urban heat-island effect leads to the ambient temperature in an urban area being higher than that in the surrounding areas.[1] This effect often generates adverse effects such as heat-stroke, discomfort, and a large consumption of electricity by air conditioners in the summer season. Natural sunlight consists of 5% ultraviolet radiation (UV; 280–400 nm), 43% visible radiation (400–700 nm) and 52% near-infrared radiation (NIR; 700–2500 nm).[2] Since the 700–1300 nm wavelength region constitutes 80% of the total energy in the NIR region, sunlight in this range plays the most important role in generating heat.[3] For this reason, it is effective to shield NIR light in this region in order to prevent heat storage. Many studies have been reported on several colored pigments that can reflect NIR light.[4–18]

The NIR-reflectance properties of variously colored pigments (*e.g.* white, yellow, and blue) are generally better than those of black pigments, because these pigments tend to reflect not only visible but also NIR light.[19,20] However, black pigments such as carbon black basically absorb NIR as well as visible light to store heat. When the common black pigment on the outer walls and roofs of buildings absorbs sunlight, the temperature rises, and at the same time the amount of exhaust heat from the use of air conditioners increases. Additionally, the heat stored during the daytime is released at night, and this heat dissipation prevents night cooling. These phenomena promote the urban heat island. For this reason, application of NIR-reflective black pigments to road surfaces, building roofs, and exterior walls has attracted attention.[20,21] Some compounds such as $(Fe, Cr)_2O_3$, Fe_2TiO_4, and $YMnO_3$ have been proposed to serve as NIR-reflective black pigments.[21–24] However, $(Fe, Cr)_2O_3$ contains toxic chromium, and NIR-reflective properties of Fe_2TiO_4 and $YMnO_3$ are not enough.

In our previous study, we found that a $Ca_2Mn_{0.85}Ti_{0.15}O_4$ pigment was a promising novel inorganic NIR-reflective black pigment.[25] But, unfortunately, this pigment exhibited slightly reddish black color. In this study, therefore, Zn^{2+} was doped into the Mn^{4+} site to improve the blackness without decreasing the NIR reflectance, because Zn^{2+} does not show optical absorption in the NIR region. Namely, $Ca_2Mn_{0.85-x}Ti_{0.15}Zn_xO_{4-x}$ ($0 \leq x \leq 0.10$) samples were synthesized and the NIR reflectance and color properties were characterized. Finally, the Zn^{2+} concentration was optimized to meet both enough black hue and high NIR reflectivity.

Experimental

Materials and methods

The $Ca_2Mn_{0.85-x}Ti_{0.15}Zn_xO_{4-x}$ ($0 \leq x \leq 0.10$) samples were synthesized using a conventional solid-state reaction method. Stoichiometric amounts of $CaCO_3$ (FUJIFILM Wako Pure

[a]Department of Chemistry and Biotechnology, Graduate School of Engineering, Tottori University, 4-101, Koyama-cho Minami, Tottori 680-8552, Japan

[b]Faculty of Engineering, Tottori University, 4-101, Koyama-cho Minami, Tottori 680-8552, Japan. E-mail: masui@tottori-u.ac.jp; Fax: +81-857-31-5264; Tel: +81-857-31-5264

[c]Center for Research on Green Sustainable Chemistry, Tottori University, 4-101, Koyama-cho Minami, Tottori 680-8552, Japan

Chemical), MnO_2 (FUJIFILM Wako Pure Chemical), TiO_2 (FUJIFILM Wako Pure Chemical), and ZnO (Kishida Chemical) were mixed in an agate mortar. The mixtures were calcined in an alumina boat at 1200 °C for 6 h under an air atmosphere. Finally, the samples were ground in an agate mortar before characterization.

Characterization

The samples synthesized were characterized by X-ray powder diffraction (XRD; Rigaku, Ultima IV) with Cu-Kα radiation (40 kV and 40 mA). The sampling width and the scan speed were 0.02° and 6 min^{-1}, respectively. The sample compositions analyzed using X-ray fluorescence spectroscopy (XRF; Rigaku, ZSX Primus) were in good agreement with the stoichiometric compositions of the starting mixtures. The lattice parameters and volumes were calculated from the XRD peak angles, which were refined using α-Al_2O_3 as a standard and using CellCalc Ver. 2.20 software. The morphology of the $Ca_2Mn_{0.85-x}Ti_{0.15}Zn_xO_{4-x}$ ($x = 0$ and 0.08) particles was investigated by using field-emission-type scanning electron microscopy (FE-SEM; JEOL, JSM-6701F). The size distribution and the average particle size were estimated by measuring the diameters of 200 particles from the FE-SEM photographs.

The optical reflectance spectra were measured with an ultraviolet-visible-near-infrared (UV-Vis-NIR) spectrometer (JASCO, V-770 with an integrating sphere attachment) with barium sulfate for the visible light region and polytetrafluoroethylene (PTFE) for the NIR region as references. The total (R_{Tot}, 300–2500 nm) and NIR (R_{NIR}, 700–2500 nm) solar reflectance was calculated in accordance with the American Society for Testing and Materials (ASTM) Standard G173-03, and was expressed as the integral of the product of the observed spectral reflectance and the solar irradiance divided by the integral of the solar irradiance, both integrated over the each range as in the formula

$$R_{Tot/NIR} = \frac{\int_{Tot/NIR}^{2500} r(\lambda)i(\lambda)d\lambda}{\int_{Tot/NIR}^{2500} i(\lambda)d\lambda}$$

where $r(\lambda)$ is the spectral reflectance obtained from the experiment and $i(\lambda)$ is the standard solar spectrum (W m^{-2} nm^{-1}). The color property was evaluated in terms of the Commission Internationale de l'Éclairage (CIE) $L^*a^*b^*C$ system using a colorimeter (Konica-Minolta, CR-300). The L^* parameter indicates the brightness or darkness of a color on relation to a neutral gray scale, and the a^* (the red-green axis) and the b^* (the yellow-blue axis) parameters express the color qualitatively. Chroma parameter (C) represents the color saturation of the pigments and is calculated according to the following formula: $C = [(a^*)^2 + (b^*)^2]^{1/2}$.

Results and discussion

X-ray powder diffraction (XRD) and field-emission-type scanning electron microscopic (FE-SEM) image

Fig. 1 shows the XRD patterns of the $Ca_2Mn_{0.85-x}Ti_{0.15}Zn_xO_{4-x}$ ($0 \le x \le 0.10$) samples. In the x range from 0 to 0.08, the target
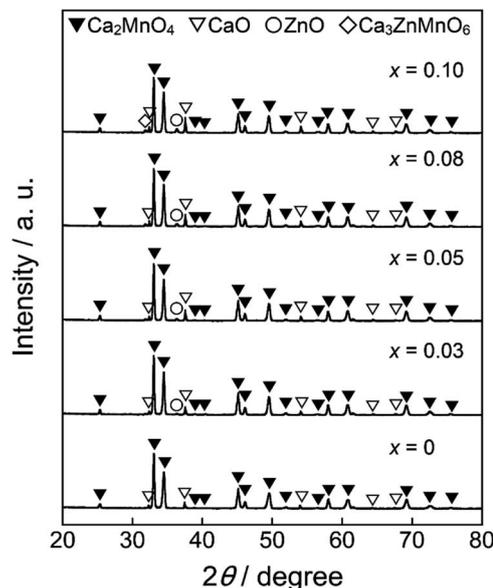

Fig. 1 XRD patterns of the $Ca_2Mn_{0.85-x}Ti_{0.15}Zn_xO_{4-x}$ ($0 \le x \le 0.10$) samples.

phase was obtained almost in a single-phase form, although nominal CaO and ZnO phases were detected. On the other hand, a small diffraction peak indexed to Ca_3ZnMnO_6 was observed at $2\theta = 32°$ as an additional impurity in the $Ca_2Mn_{0.75}Ti_{0.15}Zn_{0.10}O_{3.90}$ ($x = 0.10$) sample.

Ca_2MnO_4 forms a tetragonal structure with space group of $I4_1/acd$ (No. 142). Fig. 2 shows the crystal structure of Ca_2MnO_4 illustrated using the VESTA program[27] based on the crystallographic data reported by Leonowicz et al.[28] The [MnO_6] octahedra share corners with each other to form a two-dimensional perovskite-type array, and this [MnO_6] layer is interleaved by CaO layers in the c-axis direction. The Mn^{4+} ion in the [MnO_6] octahedron is coordinated by two $O^{2-}(1)$ ions in the c-axis direction and four $O^{2-}(2)$ ions on the ab plane. The Mn–O(1) and Mn–O(2) bond distances are 194.4 pm and 185.6 pm, respectively.[28] Accordingly, the [MnO_6] octahedron is tetragonally distorted.

The lattice parameters (a, c, and V) and the c/a ratios of all samples synthesized in this study were calculated from the XRD peak angles. These results are summarized in Table 1, where the numbers in parentheses indicate standard deviations. The cell volume increased as the Zn^{2+} concentration increased in the range of $0 \le x \le 0.08$, indicating that some Mn^{4+} (ionic radius: 53.0 pm)[26] ions were partially substituted with the larger Zn^{2+} (ionic radius: 74.0 pm)[26] ions. However, the lattice volumes of $Ca_2Mn_{0.77}Ti_{0.15}Zn_{0.08}O_{3.92}$ ($x = 0.08$) and $Ca_2Mn_{0.75}Ti_{0.15}Zn_{0.10}O_{3.90}$ ($x = 0.10$) were equal. These results indicate that the solubility limit of Zn^{2+} was approximately $x = 0.08$ in $Ca_2Mn_{0.85-x}Ti_{0.15}Zn_xO_{4-x}$.

Considering the charge compensation, the electroneutrality will be maintained by the generation of either higher valence $Mn^{5+/7+}$ or the formation of oxide anion vacancies, when Zn^{2+} is doped into the Mn^{4+} site. However, Mn^{5+} is unstable in oxides

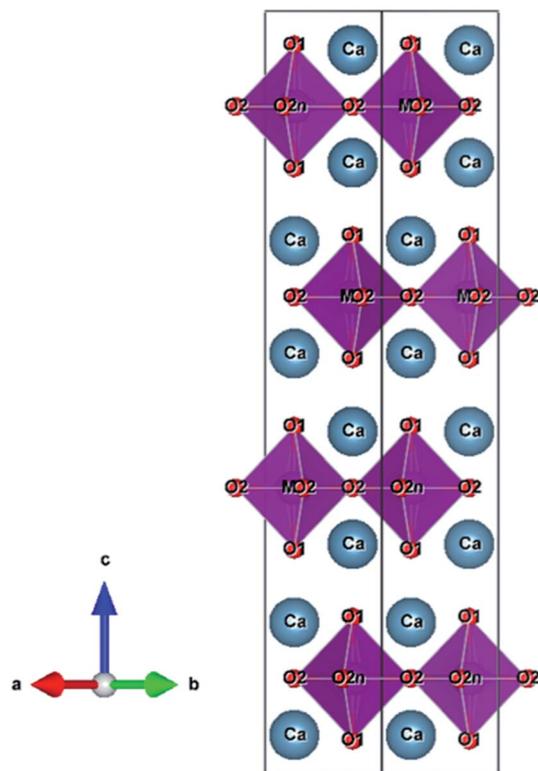Fig. 2 Crystal structure of Ca_2MnO_4.

and tends to transfer into more stable Mn^{4+} and Mn^{7+}.[29] When Mn^{7+} (ionic radius: 46 pm)[26] is generated in the structure for charge compensation, the lattice volume should increase non-linearly, but that is not the case. Therefore, it is reasonable to consider that the electrical neutrality of $Ca_2Mn_{0.85-x}Ti_{0.15}Zn_x$-$O_{4-x}$ is maintained by the production of oxide anion vacancies.

The lattice parameters a and c also increased with increasing the Zn^{2+} content. However, the increase rates of the former and the latter were different. The crystal structure of $Ca_2(Mn, Nb)O_4$ was investigated by Taguchi.[30] When the Nb^{5+} ions were introduced into the Mn^{4+} site in Ca_2MnO_4, the c/a ratio decreased with increasing the Nb^{5+} content, and the distortion of the $[MnO_6]$ octahedra was alleviated.[30] On the contrary, in the case of the $Ca_2Mn_{0.85-x}Ti_{0.15}Zn_xO_{4-x}$ ($0 \leq x \leq 0.10$) samples synthesized in this study, the c/a ratio increased with increasing the amount of Zn^{2+} in the range of $0 \leq x \leq 0.05$, as seen in Table 1. Therefore, the distortion of the $[MnO_6]$ octahedra was increased by the partial substitution of Mn^{4+} with Zn^{2+}.

Table 1 Lattice parameters (a, c, and V) and c/a ratio of the Ca_2-$Mn_{0.85-x}Ti_{0.15}Zn_xO_{4-x}$ ($0 \leq x \leq 0.10$) samples

x	a/nm	c/nm	c/a	V/nm^3
0	0.52084(7)	2.4121(4)	4.6312(10)	0.6543(2)
0.03	0.52091(12)	2.4140(9)	4.634(2)	0.6550(4)
0.05	0.52096(10)	2.4159(7)	4.637(2)	0.6557(3)
0.08	0.52110(12)	2.4167(8)	4.638(2)	0.6562(4)
0.10	0.5211(2)	2.4168(12)	4.638(3)	0.6562(6)

Fig. 3 shows the FE-SEM images and size distributions of the $Ca_2Mn_{0.85-x}Ti_{0.15}Zn_xO_{4-x}$ ($x = 0$ and 0.08) samples. The faceted particles were observed in both samples. These particles were thermally fused due to the high-calcination temperature at 1200 °C. In both samples, the average particle size was 0.97 μm and there was no significant change in particle size, size distribution, and morphology. These results indicate that the changes in the optical and color properties of both samples were caused by the Zn^{2+} doping.

Reflectance spectra

Fig. 4(a) depicts the UV-Vis and NIR reflectance spectra of the $Ca_2Mn_{0.85-x}Ti_{0.15}Zn_xO_{4-x}$ ($0 \leq x \leq 0.10$) samples. All samples strongly absorbed visible light at a wavelength of 700 nm and shorter and reflected NIR light, due to small bandgap energies around 1.77 eV.[25] An enlarged view of the reflectance spectra from 300 to 750 nm was shown in Fig. 4(b). Optical reflectance from 600 to 750 nm corresponding to the red light was decreased by the Zn^{2+} doping. As a result, the color of the samples changed from slightly reddish black to more vivid black and the redness of the samples was reduced.

As discussed above in Table 1, the $[MnO_6]$ octahedron was significantly distorted by the dissolution of Zn^{2+}. This lattice distortion increased with increasing the Zn^{2+} concentration, and the symmetry of the $[MnO_6]$ octahedron decreased. Thus, the reduction in red light reflection was caused by the d–d transition absorption of Mn^{4+}. This transition is essentially forbidden but has been partially allowed due to the loss of symmetry. On the other hand, the Mn^{4+} content of the sample was decreased by the Zn^{2+} substitution. In other words, enhancement of the optical absorption by Mn^{4+} in the red-light region and decrease of the amount of Mn^{4+} responsible for this absorption are in the relationship of trade-off. Accordingly, the optical reflectance in the red-light region almost unchanged in the range of $0.03 \leq x \leq 0.08$.
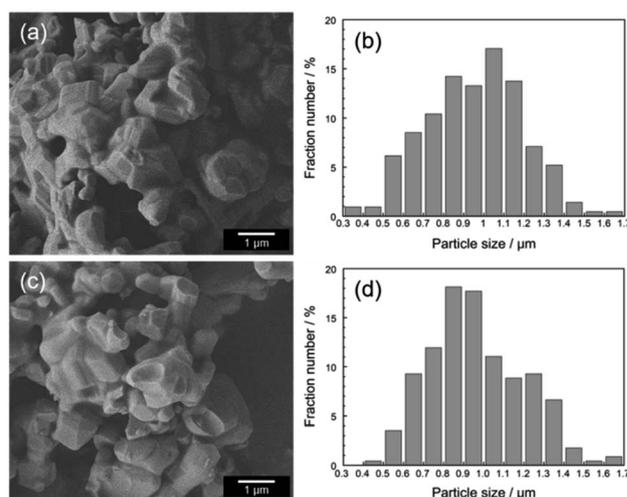

Fig. 3 FE-SEM images and size distributions of $Ca_2Mn_{0.85}Ti_{0.15}O_4$ (a and b) and $Ca_2Mn_{0.77}Ti_{0.15}Zn_{0.08}O_{3.92}$ (c and d).
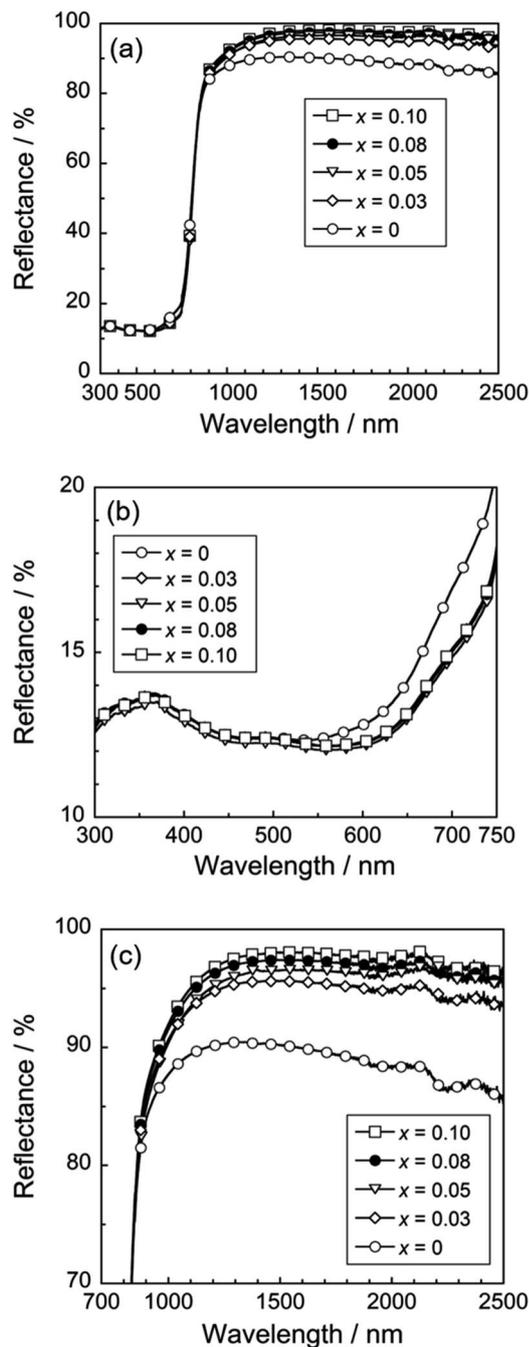
Fig. 4 UV-Vis-NIR (a), UV-Vis (b), and NIR (c) reflectance spectra of the $Ca_2Mn_{0.85-x}Ti_{0.15}Zn_xO_{4-x}$ ($0 \leq x \leq 0.10$) samples.

On the other hand, the optical reflectance in the NIR region was increased by the Zn^{2+} doping, as seen in Fig. 4(c). The optical absorption in the NIR region was caused by the allowed charge transfer transition between Mn^{4+} and Mn^{3+} ions,[31] and this absorption intensity depended on the concentration of manganese. Unfortunately, it is difficult to confirm how much the CaO and ZnO impurity phases are involved in improving the NIR reflectivity. Since CaO and ZnO can strongly reflect the visible light as well as the NIR light, the optical reflectance in the visible light region shall also be increased by the Zn^{2+}

doping, when the effect of these impurities is large. However, the reflectance in the visible light region did not increase, but rather the reflectance of red light decreased. Therefore, the increase in the NIR reflectivity is dominantly due to the decrease in manganese ions in the sample.

Chromatic properties and NIR solar reflectance

The color coordinate data and total (R_{Tot}) NIR solar reflectance (R) of the $Ca_2Mn_{0.85-x}Ti_{0.15}Zn_xO_{4-x}$ ($0 \leq x \leq 0.10$) pigments are summarized in Table 2. The photographs of these pigments are also displayed in Fig. 5. All pigments synthesized in this study showed low L^* values and were black as seen in Fig. 5. The a^*, b^*, and C values of the Zn^{2+}-doped pigments were almost the same, but lower than those of the undoped $Ca_2Mn_{0.85}Ti_{0.15}O_4$ pigment ($x = 0$). As already discussed with respect to the results in Fig. 4(b), this was due to the decrease in the optical reflection in the red-light region (600–750 nm). The R value increased conversely with the Zn^{2+} doping, because the relative number of manganese ions decreased and the reflectance in the NIR region was increased as seen in Fig. 4(a) and (c).

For an achromatic color such as black, the C value should be as small as possible in the $L^*a^*b^*C$ system. As recognized in the C and R_{NIR} values of the Zn^{2+}-doped samples in Table 2, the color tone became blacker and the NIR solar reflectance was improved. Among the $Ca_2Mn_{0.85-x}Ti_{0.15}Zn_xO_{4-x}$ ($0 \leq x \leq 0.08$) pigments synthesized in this study, $Ca_2Mn_{0.77}Ti_{0.15}Zn_{0.08}O_{3.92}$ showed a relatively low C value and the highest R_{NIR} value. Therefore, it was evidenced that $Ca_2Mn_{0.77}Ti_{0.15}Zn_{0.08}O_{3.92}$ has high performance as an inorganic black pigment with thermal barrier characteristics.

Comparison with commercially available pigments

The UV-Vis-NIR reflectance spectrum and the color parameters of the $Ca_2Mn_{0.77}Ti_{0.15}Zn_{0.08}O_{3.92}$ pigment was compared with those of the commercially available black pigments such as Black 6350 (iron and chromium oxide, Asahi Kasei), Black 6301 (manganese and bismuth oxide), MPT-370 (calcium, manganese, and titanium oxide, Ca(Ti, Mn)O₃, Ishihara Sangyo), and carbon black (Wako Chemical), as shown in Fig. 6 and summarized in Table 3. The photographs of these pigments are also displayed in Fig. 7. As evidenced from these results, the present $Ca_2Mn_{0.77}Ti_{0.15}Zn_{0.08}O_{3.92}$ pigment showed higher reflectance in the NIR wavelength region and significantly higher R_{NIR} value than did the commercial pigments. Furthermore, the present pigment showed sufficiently low L^* and C

Table 2 Color coordinate data and total (R_{Tot}) and NIR (R_{NIR}) solar reflectance of the $Ca_2Mn_{0.85-x}Ti_{0.15}Zn_xO_{4-x}$ ($0 \leq x \leq 0.10$) pigments

x	L^*	a^*	b^*	C	R_{Tot}/%	R_{NIR}/%
0	24.4	+4.30	+2.72	5.09	43.7	71.7
0.03	23.2	+2.70	+0.72	2.79	44.6	73.8
0.05	22.1	+2.84	+0.94	2.99	44.5	73.7
0.08	23.2	+2.81	+0.83	2.93	45.0	74.6
0.10	23.3	+2.97	+0.94	3.12	45.3	75.1
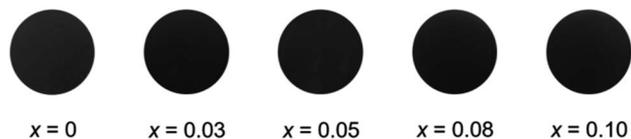
Fig. 5 Photographs of the $Ca_2Mn_{0.85-x}Ti_{0.15}Zn_xO_{4-x}$ ($0 \leq x \leq 0.10$) pigments.

Fig. 7 Photographs of $Ca_2Mn_{0.77}Ti_{0.15}Zn_{0.08}O_{3.92}$ (a), Black 6350 (b), Black 6301 (c), MPT-370 (d), and carbon black (e).
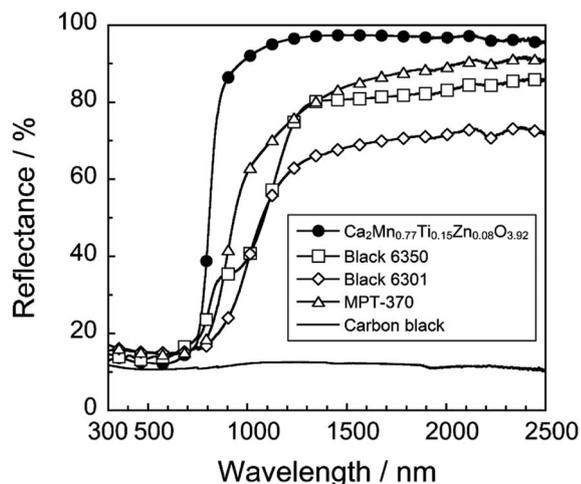

Fig. 6 UV-Vis-NIR reflectance spectra of various black pigments.

Table 4 Color coordinates and total (R_{Tot}) and NIR (R_{NIR}) solar reflectance of $Ca_2Mn_{0.77}Ti_{0.15}Zn_{0.08}O_{3.92}$ before and after chemical stability test

Treatment	L^*	a^*	b^*	C	R_{Tot}/%	R_{NIR}/%
Non-treatment	23.2	+2.81	+0.83	2.93	45.0	74.6
4% CH_3COOH	16.0	+10.6	+3.33	11.1	39.4	63.8
4% NH_4HCO_3	23.6	+4.76	+4.32	6.43	44.4	73.0

with a stable compound such as silica is necessary to suppress the deterioration.

values, similar to the vcommercially available NIR-reflective black pigments.

Conclusions

$Ca_2Mn_{0.85-x}Ti_{0.15}Zn_xO_{4-x}$ solid solutions were synthesized as NIR-reflective black pigments to improve the blackness of a $Ca_2Mn_{0.85}Ti_{0.15}O_4$ pigment without decreasing the NIR reflectance. By the introduction of Zn^{2+} in the $Ca_2Mn_{0.85}Ti_{0.15}O_4$ lattice, the reflection of the red-light (600–750 nm) was decreased due to the enhancement of the d–d transition of Mn^{4+}, while the NIR reflectance was increased by the decrease of the charge transfer transition between Mn^{4+} and Mn^{3+}. As a result, the black color tone of the non-doped $Ca_2Mn_{0.85}Ti_{0.15}O_4$ pigment was improved by the Zn^{2+} doping, and the highest NIR solar reflectance value (R_{NIR} = 74.6%) was observed at the composition of $Ca_2Mn_{0.77}Ti_{0.15}Zn_{0.08}O_{3.92}$. Furthermore, the present pigment exhibited enough black color and the NIR reflectance ability is significantly higher than those of the conventional commercially available black pigments (R_{NIR} < 53.0%). Although it is necessary to improve the chemical stability, the $Ca_2Mn_{0.77}Ti_{0.15}Zn_{0.08}O_{3.92}$ pigment has a potential to be an inorganic black pigment for thermal shielding.

Chemical stability test

The chemical stability of the $Ca_2Mn_{0.77}Ti_{0.15}Zn_{0.08}O_{3.92}$ pigment was also evaluated. The powder sample was soaked into 4% acetic acid and 4% ammonium bicarbonate aqueous solutions. After leaving them at room temperature for 24 h, the samples were washed with deionized water and ethanol, and then dried at room temperature. The NIR-reflectance properties and color of the samples after the chemical stability test was evaluated using the UV-Vis-NIR spectrometer and the colorimeter. Unfortunately, the color degradation and the decrease of the R_{Tot} and R_{NIR} values were observed by leaching the sample in both acetic acid and basic ammonium carbonate solutions, as seen in Table 4. Therefore, it is suggested that surface coating

Conflicts of interest

There are no conflicts to declare.

Table 3 Color coordinate data and total (R_{Tot}) and NIR (R_{NIR}) solar reflectance of the black pigments

Pigment	L^*	a^*	b^*	C	R_{Tot}/%	R_{NIR}/%
$Ca_2Mn_{0.77}Ti_{0.15}Zn_{0.08}O_{3.92}$	23.2	+2.81	+0.83	2.93	45.0	74.6
Black 6350	26.4	+0.93	+4.19	4.29	31.7	47.8
Black 6301	24.0	+0.77	+1.14	1.38	28.3	40.3
MPT-370	25.1	+0.90	−0.41	0.99	34.5	52.3
Carbon black	2.69	+0.98	+1.90	2.14	11.3	11.7

References

1 H. Akbari, *Urban Heat Islands: Consequences and Mitigation Measures*, Springer, 2015.

2 R. Levinson, P. Berdahl and H. Akbari, *Sol. Energy Mater. Sol. Cells*, 2005, **89**, 319.

3 B. Kaur, N. Quazi, I. Ivanov and S. N. Bhattacharya, *Dyes Pigm.*, 2012, **92**, 1108.

4 Y. Shi, M. Zhong, Z. Zhang and D. Wang, *Ceram. Int.*, 2017, **43**, 5979.

5 B. Huang, Y. Xiao, H. Zhou, J. Chen and X. Sun, *ACS Sustainable Chem. Eng.*, 2018, **6**, 10735.

6 C. Ding, A. Han, M. Ye, Y. Zhang, L. Yao and J. Yang, *RSC Adv.*, 2018, **8**, 19690.

7 T. R. A. Thara, P. P. Rao, A. K. V. Raj and T. S. Sreena, *Sol. Energy Mater. Sol. Cells*, 2019, **200**, 110015.

8 S. F. Sameera, P. P. Rao, L. S. Kumari, V. James and S. Divya, *Chem. Lett.*, 2013, **42**, 521.

9 S. Jose, S. B. Narendranath, D. Joshy, N. V. Sajith, M. R. P. Kurup and P. Periyat, *Mater. Lett.*, 2018, **233**, 82.

10 B. Huang, Y. Xiao, C. Huang, J. Chen and X. Sun, *Dyes Pigm.*, 2017, **147**, 225.

11 J. Chen, Y. Xiao, B. Huang and X. Sun, *Dyes Pigm.*, 2018, **154**, 1.

12 P. K. Thejus, B. Koley and K. G. Nishanth, *Dyes Pigm.*, 2018, **158**, 267.

13 E. A. Chavarriaga, A. A. Lopera, T. B. Wermuth, O. J. Restrepo and C. P. Bergmann, *Dyes Pigm.*, 2018, **157**, 1.

14 A. K. V. Raj, P. P. Rao, S. Divya and T. R. Ajuthara, *Powder Technol.*, 2017, **311**, 52.

15 B. Bae, N. Takeuchi, S. Tamura and N. Imanaka, *Dyes Pigm.*, 2017, **147**, 523.

16 J. Jing, Y. Zhang, J. Sun, X. Zhao, D. Gao and Y. Zhang, *Dyes Pigm.*, 2018, **150**, 9.

17 M. Cai, S. Chen, X. Ma and J. Chen, *J. Rare Earths*, 2019, **37**, 741.

18 J. O. Primo, K. W. Borth, D. C. Peron, V. C. Teixeira, D. Galante, C. Bittencourt and F. J. Anaissi, *J. Alloys Compd.*, 2019, **780**, 17.

19 R. Levinson, P. Berdahl and H. Akbari, *Sol. Energy Mater. Sol. Cells*, 2005, **89**, 351.

20 R. Levinson, P. Berdahl, H. Akbari, W. Miller, I. Joedicke, J. Reilly, Y. Suzuki and M. Vondran, *Sol. Energy Mater. Sol. Cells*, 2007, **91**, 304.

21 S. Jose, D. Joshy, S. B. Narendranath and P. Periyat, *Sol. Energy Mater. Sol. Cells*, 2019, **194**, 7.

22 E. B. Faulkner and R. J. Schwartz, *High Performance Pigments*, Wiley–VCH, 2nd edn, 2009.

23 A. Han, M. Zhao, M. Ye, J. Liao, Z. Zhang and N. Li, *Sol. Energy*, 2013, **91**, 32.

24 A. Han, M. Ye, M. Zhao, J. Liao and T. Wu, *Dyes Pigm.*, 2013, **99**, 527.

25 R. Oka and T. Masui, *RSC Adv.*, 2016, **6**, 90952.

26 R. D. Shannon, *Acta Crystallogr., Sect. A: Cryst. Phys., Diffr., Theor. Gen. Crystallogr.*, 1976, **32**, 751.

27 K. Momma and F. Izumi, *J. Appl. Crystallogr.*, 2011, **44**, 1272.

28 M. E. Leonowicz, K. R. Poeppelmeier and J. M. Longo, *J. Solid State Chem.*, 1985, **59**, 71.

29 E. A. Medina, J. Li, J. K. Stalick and M. A. Subramanian, *Solid State Sci.*, 2016, **52**, 97.

30 H. Taguchi, *Mater. Res. Bull.*, 2001, **36**, 1361.

31 N. N. Kovaleva, J. L. Gavartin, A. L. Shluger, A. V. Boris and A. M. Stoneham, *J. Exp. Theor. Phys.*, 2002, **94**, 178.